An optimization technique for addressing DEM misregistration

Wenwen Li and Michael F. Goodchild
Center for Spatial Studies
University of California, Santa Barbara
Santa Barbara, CA, 93106-4060
{wenwen,good}@geog.ucsb.edu

Description

A spatial optimization technique is proposed to quantify the misregistration between 30m SRTM and NED dataset in the mountainous regions in Los Angeles County, CA, US.

Abstract

DEMs represent Earth's topography and support a variety of applications, ranging from extracting watershed drainage structure to measuring glacier volume. Applications which require conflation of multiple DEMs are problematic, however, because of misregistration. We explore a spatial optimization technique to quantify the misregistration on the pixel level between NASA's SRTM elevation dataset and the USGS'S NED. The misregistration, estimated by horizontal offset and direction, is modeled spatially in terms of typical topographical parameters: slope, aspect, and elevation. A Nelder-Mead algorithm was implemented to compute the local shift at two study sites in the San Gabriel Mountains (SGM) and Santa Monica Mountains (SMM) in Los Angeles County, CA. It was found that the magnitude of misregistration is generally less than the distance between DEM postings, and that the magnitude varies by terrain type, being larger in steeper terrains; nevertheless, misregistration is systematic within continuous terrains that have similar topographical features.

Keywords: Spatial optimization, Digital elevation model, Nelder-Mead algorithm, Accuracy assessment, Registration, Spatial modeling

1. Introduction

Recent years have seen a proliferation of digital elevation data, largely as a result of new acquisition systems. Digitized contours are often obtained by scanning published topographic maps, or acquired as an intermediate product in the mapping process. Rasters of elevation data are often used in geographic applications and analysis. These datasets are often found in the form of: digital elevation models (DEMs), through interpolation from contours (the contour-to-grid or CTOG process), by remote sensing using radar (*e.g.* Shuttle Radar Topography Mission or SRTM data) or LiDAR data, or by interpolation from spot heights. The resulting data sets will vary by spatial resolution and the measurement accuracy of position and elevation, and also by semantics, or precisely what is meant by height. LiDAR first returns, for example, will record the elevation of the tree canopy or buildings; radar will also be affected by dense canopies and buildings (DEMs acquired from LiDAR or radar are sometimes termed digital *surface* models or DSMs for this reason); and the elevations depicted on topographic maps are typically those of the bare ground devoid of buildings, trees, and in some cases sand dunes (bare-earth DEMs obtained from topographic maps are sometimes termed digital *terrain* models, or DTMs). Some DEMs record the elevation measured at point locations, while in other cases the elevation reported may be the average over a pixel, or the result of a more complex spatial convolution.

This variety of elevation data is opening new applications that rely on the ability to fuse or compare two or more sources. Our study, for example, is motivated by a need to estimate the spatial distribution of building volume in Los Angeles, and our exploration of the possibility to accomplish this by comparing a DEM that records the elevation of bare ground with one, specifically SRTM, that records the top surface of any buildings that are present. This effort required a careful registration of the two DEMs; this paper reports on the technique we developed

to address that problem. The broader issue of building volume estimation will be addressed in a separate paper. Besides the application of DEMs in our study, a number of other scientific research topics, such as extraction of watershed drainage structure (Maddalena, 2010), estimation of canopy height (Miliaresis and Delikaraoglou, 2009) and measurement of glacier volume (Nuth and Kaab, 2011), all need cross-source DEM analysis. To perform precise science, it is imperative that the misregistration across DEMs are identified and corrected.

In some cases it is possible to address misregistration visually, or at least to gain some rough impression of its amount and direction. For example, in the Ridge and Valley Province of the Appalachian Mountains, an offset between two DEMs that is perpendicular to the ridges would lead to a characteristic pattern that alternates positive and negative elevation errors. Figure 1a shows an area near Harrisonburg, VA (79 to 80 degrees West, 38 to 39 degrees North), where the ridges run approximately southwest to northeast. We created two copies of a DEM, and offset one copy perpendicular to the ridges by a distance of 0.83 pixels. To make the offset DEM aligned with the sample points in the original dataset, the following resampling strategy was introduced:1) Each pixel in the original DEM was re-sampled to 7*7 equal-size pixels of the same value, so the size of each new pixel is 1/7th that of the original pixel. 2) The new DEM was moved 5 new pixels to the east and 3 new pixels to the south, making the absolute shift $\mathrm{sqrt}((5/7)^2+(3/7)^2)$, or 0.83, original pixels. Figure 1b shows the result of differencing the two sets of elevations. Along each mountain ridge, the differences are all negative (black) on the northwest facing slope of the ridge, and positive on the southeast slope, allowing the ridges and valleys to become clear, as if the surface were illuminated from the southeast.

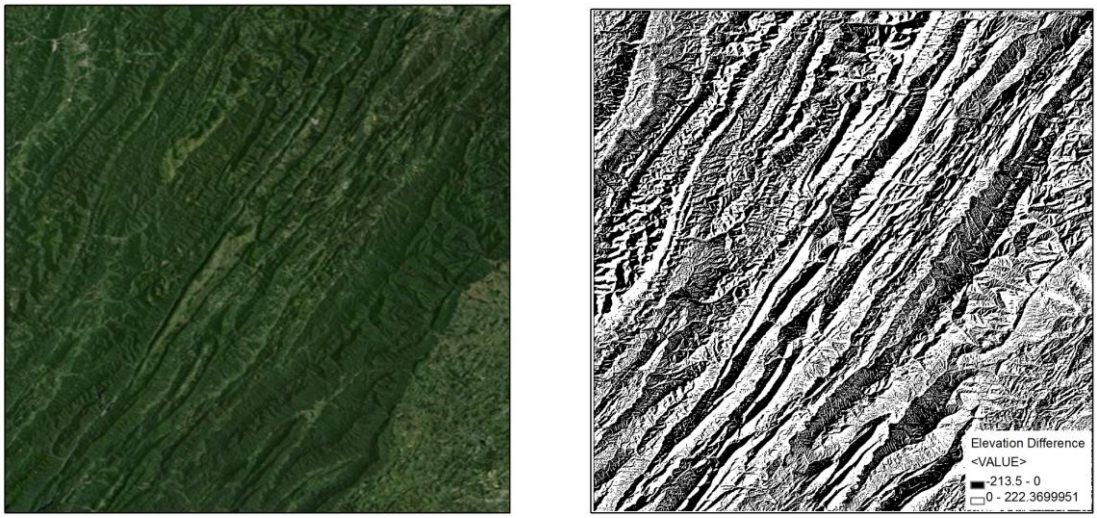

(a) (b)

Figure 1 (a) Satellite imagery of Appalachian Mountains ranges near Harrisonburg, VA (b) Elevation differences between a DEM and an offset copy over the same region.

The Appalachian Mountains example is an ideal case illustrating the patterns caused by sub-pixel misregistration because (1) these mountains are mostly single-directional; (2) we impose a constant shift in a single direction perpendicular to the structure of the mountain range. Therefore, the misregistration can be detected easily. However, in real-world situations, the identification of misregistration is much more complicated. It is therefore essential to develop a computer-aided spatial model for automated misregistration detection. The rest of the paper is organized as follows. Section 2 introduces the related research in the literature, Section 3-5 describe the study area, dataset in use, and the proposed method, Section 6 presents experimental results from case studies, and Section 7 concludes the paper and points out future research directions.

2. Literature

In image processing it is sometimes necessary to fuse two or more images that have been produced by different approaches, acquired at different times, or acquired from different points of

view (Zitová and Flusser, 2003). In such cases it is desirable to remove any misregistration that may be present, using one of two traditional methods. The *feature-matching* method involves computing the cross-correlation for a range of distances and directions between the image to be registered and a reference image, and selecting the distance and direction for which cross-correlation is maximum (Reddy and Chatterji, 1996; Guizar-Sicairos, Thurman and Fienup., 2008). *Transform-model estimation* involves the identification of a number of control points, on both the image to be registered and the reference image, that can be used to warp one to fit the other. Global approaches such as shape-perserving mapping and local approaches such as thin-plate splines (Davis *et al.*, 1997) are commonly used transform models.

Most of the image registration studies reported in the literature focused on registering images that exhibit sharp changes of value. Land-cover images, for example, have values that change sharply at the edges of different land-cover types, and may be classified, in which case values are measured on nominal scales. In contrast, elevation surfaces are measured on interval scales and typically follow Tobler's First Law of Geography (Sui, 2004), exhibiting strong spatial autocorrelations over short distances. Moreover some acquisition methods tend to lead to misregistrations that are sensitive to the spatial structure of the terrain. These two characteristics of DEM data pose great challenges in the registration of such datasets from multiple sources.

One popular method of measuring the positional accuracy of a DEM and improving its registration is by using ground control points (GCPs). The basic procedure is to: (1) identify a set of GCPs and measure their locations; (2) obtain the elevation at the GCP from in-situ measurement or from an independent source that is known to have better accuracy (Maune *et al.*, 2007); (3) identify feature points to be matched on the DEM; (4) estimate the parameters of a 3D transformation using the matched point pairs, with the objective of minimizing the least-square error of the elevations. However, this method is not effective for large-scale terrain DEM

registration because it is costly and time consuming, and it may occasionally be impossible to obtain enough GCPs (Goodchild *et al.*, 1994; Zebker *et al.*, 1994). Moreover, if the number of GCPs is limited and the transform model is poorly chosen, the result may be large discrepancies between the transformed DEM and the reference source, even after transformation (Carpenter and Hogarty, 2007).

To overcome this drawback, researchers have investigated the capabilities of DEM to DEM registration utilizing all of the available terrain information (Carpenter and Hogarty, 2007; Dawn, *et al.*, 2010). Carpenter and Hogarty performed a simultaneous vertical and horizontal DEM registration using a "coarse exhaustive" algorithm, a "coarse with parabolic refinement" algorithm, and a "unified least squares" algorithm. The objective was to find the best fit between the master DEM (finer-resolution DEM) and the DEM to be registered (coarser-resolution DEM). This study found that the shift obtained is more reliable using DEMs with similar resolutions than with very different resolutions. It was not mentioned whether the complexity of terrains, such as local slope and aspect, were considered in the registration.

Recently, sub-pixel misregistration of images has attracted much attention. Dai and Khorram (1998) showed that highly accurate change detection (with less than 10% error induced) based on multi-temporal Landsat Thematic Mapper (TM) images requires that the magnitude of misregistration be less than 0.2 pixel (see also Townshend et al., 1992), in other words, less than 0.2 times the horizontal separation of DEM postings. Simard (2006) reported an instance of sub-pixel DEM misregistration. Van Niel et al. (2008) investigated the impact of misregistration between DEMs, including SRTM, and found that differences between DEMs are very sensitive to sub-pixel misregistration, and that the sensitivity depends on the pixel sizes of the datasets being compared (see also Smith and Sandwell, 2003). They also concluded that even low levels of misregistration caused considerable differences in landscapes with steep terrains. However,

neither of the above studies quantified the actual misregistration between different DEM sources. In this paper, we report on our efforts to design a spatial model that considers two important topographic parameters, slope and aspect, to quantify the misregistration (we also term it the shift) in our study areas. The model is solved using optimization techniques (introduced in Section 5.2) and the shift is quantified in terms of the horizontal distance and direction of offset. Once the misregistration is corrected, any systematic differences in elevations between the two data sets can be evaluated.

3. Study Sites

Two study sites in Los Angeles County in Southern California area were selected for this study: one located in the San Gabriel Mountains in the north of the county, and the other in the Santa Monica Mountains in the southwest, as Figure 2 (a) shows. These two mountainous regions were selected because there are few developments in the regions, therefore, the elevation difference between DSM such as SRTM and DTM such as NED (National Elevation Dataset) would be minimal. The study site SGM (black box in Figure 2.b) in the San Gabriel Mountain region is 153km^2, covering a geographic extent of [-118.38 °, 34.34 °, -118.19 °, 34.42 °]. It has very steep terrain, the distribution of slopes (slope defined as vertical rise over horizontal run, that is, the tangent of the slope angle) having a mean of 50% and a standard deviation of 22%. The elevations in this area lie between 568m and 1845m (mean = 1145m; standard deviation = 249.5m). The study site SMM (black box in Figure 2.c) in the Santa Monica Mountain region is 274km^2, covering a geographic extent of [-118.86 °, 34.04 °,-118.56 °, 34.13 °]. Although less steep than SGM, the SMM region also has relatively steep terrain, with a mean slope of 38% (standard deviation 21%). The maximum and minimum elevations of this site are 3.2m and 860m respectively. The mean elevation is 374m, with a standard deviation of 146.8m.


45°0'0"N
40°0'0"N
35°0'0"N
120°0'0"W
Montana
Oregon
Idaho
Nevada
Utah
California
Arizona
SGM
SMM

(a)

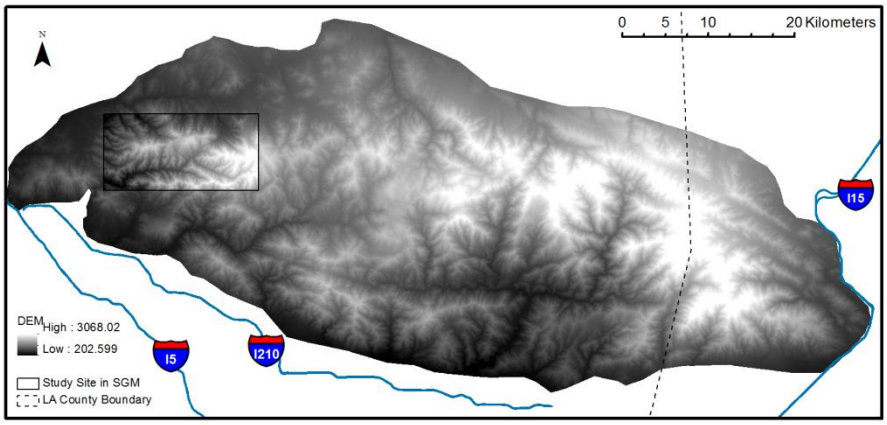
N
0 5 10 20 Kilometers
I15
I5
I210
DEM
High : 3068.02
Low : 202.599
Study Site in SGM
LA County Boundary

(b)

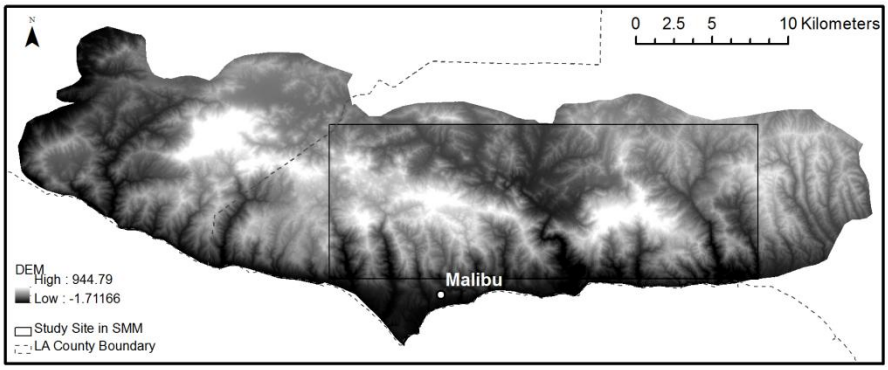
N
0 2.5 5 10 Kilometers
Malibu
DEM
High : 944.79
Low : -1.71166
Study Site in SMM
LA County Boundary

(c)

Figure 2. (a) The regional placement of the study sites. (b) and (c) The topography of the San Gabriel Mountain region (b) and the Santa Monica Mountain region (c) from the NED DEM (the black rectangles indicate the study areas).

4. Data

The Shuttle Radar Topography Mission, an international effort led by the U.S. National Geospatial-Intelligence Agency and the U.S. National Aeronautics and Space Administration, was carried out between Feb. 11th and Feb. 22nd 2000. A C/X-band Synthetic Aperture Radar (SAR) was carried on board the space shuttle endeavor, and used to scan the Earth's surface elevation between 54 ° South and 60 ° North. The radar signal was reflected off the first object encountered, and was therefore affected by all constructed or natural objects on the Earth's surface. For this reason, the SRTM data could be categorized as a digital surface model (DSM).

The SRTM Version 2 data were released in 2005, with certain artifacts fixed, including single-pixel errors and the noise that occurs in radar returns from water surfaces. The 3 arc-second (approximately 90m) and 1 arc-second (approximately 30m) data are downloadable from USGS's seamless data warehouse (http://seamless.usgs.gov) in 1 °by 1 °tiles. 3 arc-second SRTM data are available for most of the world's continents, but 1 arc-second SRTM data are publicly available only for the USA. The specifications of SRTM data are provided in Table1.

In this study, the NED data were used as the reference data, comparing to which the shift of SRTM would be indentified. NED data are generated from the bare-earth contours of USGS 1:24,000-scale topographic maps. The contours are then gridded at a constant spacing into quadrangle-based DEM tiles (Gesch *et al.* 2003; Gesch, 2007). Each tile is clipped to the actual coverage extent (1^o by 1^o) to remove edge artifacts. The NED data are available at 3 arc-second, 1 arc-second, and 1/3 arc-second postings on USGS's seamless data warehouse.

Basing DEM points on equal intervals of latitude and longitude necessarily leads to east-west spacings that are only 83% of north-south spacings at the latitude of Los Angeles. For the purposes of this study, we reprojected both data sets to UTM Zone 11, resampling both to a spacing of 27.24m to ensure that the DEM points are equidistant in both directions. In principle the postings of the two data sets should coincide, though the implicit convolution functions are different - NED data are more point-like, with narrow convolution functions, while the SRTM elevations compare better to averages over pixel areas because of the wider implicit convolutions.

Table 1 shows the published profiles of the two data sets.

DEM Source	NED	SRTM
Full name	National Elevation Data	Shuttle Radar Topography Mission
Provider	USGS	NASA
Type	Bare-earth elevation	Surface elevation
Spatial resolution	1/3 arc second (~10m) 1 arc second (~30m) 3 arc-second (~90m)	1 arc second (~30m) 3 arc second (~90m)
Vertical accuracy	2.44m (Gesch *et al.*, 2002)	9.0m (Rodr ́guez *et al.*, 2006)
Horizontal accuracy	±5m	±20m (90% confidence level)

5. Methods

5.1 Problem formulation

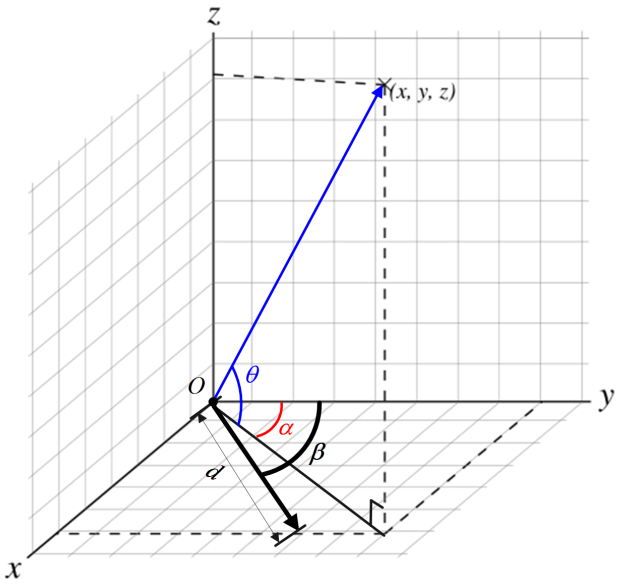

Figure 3. Vector representation of local shift $\vec{D} = (d, \beta)$ in three-dimensional space. y axis towards North, x axis towards the East and z axis measures the elevation above ground. d is the offset of the shift and β is the direction of the shift measured clockwise from North. The terrain slope is represented by an inclination θ to the horizontal, and aspect is represented by an angle α measured closewise from North.

This section presents a formal mathematical representation of the components (slope, aspect, elevation, shift offset and shift angle) that influence the multi-source DEM differencing process. Consider the same point P in both SRTM and NED DEMs. The shift from SRTM to NED is a vector $\vec{D}$, represented by its offset d and direction β, as Figure 3 shows. Let ε^* denote the difference in elevations provided at a point by the two sources, and let ε denote the error that would be observed at that point due to a misregistration of amount $\vec{D}$ alone. When $\beta = \alpha$, the shift is in the direction of steepest slope, and because of misregistration the elevations obtained from the two sources should differ by $d \tan\theta$, plus any error due to mismeasurement. When

$\beta \neq \alpha$, the apparent slope parallel to β is $\tan\theta\cos(\beta-\alpha)$, therefore, the misregistration error caused by the shift equals:

$$\varepsilon = d\tan\theta\cos(\beta-\alpha)$$

Our objective is to identify the unknowns d and β.

We assume that d and β vary slowly, and can be estimated using a block strategy. For example, a block of 1 sq km contains about 900 observations, and can be used to estimate the shift parameters over the block. Writing the problem as an optimization, the objective can be formalized as:

$$\text{Minimize } \sum_{i=1}^{n}\left(\varepsilon_i - \varepsilon_i^*\right)^2 = \sum_{i=1}^{n}\left[d_i \tan\theta_i \cos\left(\beta_i - \alpha_i\right) - \varepsilon_i^*\right]^2,$$

where n is the number of observations that fall inside the desired scene. Note that we assume a local shift for each block instead of a single global shift because the former emphasizes the effects of local geometric features (Flusser, 1992; Goshtasby, 1987), though we expect some degree of consistency in the estimates for each block. In the next section, the methods used for the shift estimation will be discussed.

5.2 Multidimensional unconstrained nonlinear minimization

The following characteristics of the objective function indicate that this problem can be categorized as a multidimensional unconstrained nonlinear optimization problem. First, the minimization of the objective function is decided by more than one variable (d and β), meaning that the problem space is multi-dimensional. Second, the objective function is non-linear since it is twice continuously differentiable. Third, the domain of permissible solutions is not limited to variables satisfying some equality or inequality constraints, therefore it is an unconstrained problem.

In the literature, there are many methods and algorithms developed to solve the multidimensional unconstrained nonlinear problem, such as Newton's method, Broyden's method (Broyden, 1965), line-search methods, trust-region methods (Celis *et al.*, 1985), the Nelder-Mead simplex method (Nelder and Mead, 1965), the conjugate-gradient method (Hestenes and Stiefel, 1952), and their variants (Fan and Zahara, 2007; Birgin and Martinez, 2001; Neculai, 2008). Most of these algorithms involve an iterative process that converges on a sufficiently accurate solution. Newton's method is a typical example of the above processes. However, the method is very computational intensive ($O(n^{\wedge 3})$ operations per iteration) and requires many function evaluations at each iteration. Broyden's method does not require the error-prone computation in Newton's method and it is able to reduce the computational complexity from $O(n^{\wedge 3})$ to $O(n^{\wedge 2})$. But it may fail to converge on the optimal solution if poor starting points are selected. In comparison, line-search methods and trust-region methods introduce strategies, such as steepest descent (Wolfe, 1969), to prevent the process from getting stuck at a local optimum, while preserving the advantages of local convergence as Newton's and Broyden's method do. All of these methods are derivative-dependent and are therefore computational intensive. To overcome this drawback, the direct-search methods are built on sound heuristics and are derivative-free. Methods such as the Nelder-Mead algorithm and the conjugate-gradient method have drawn a lot of attention in the optimization field (Dennis and Schnabel, 1989; Lewis *et al.*, 2000). The conjugate-direction method is more suitable for solving problems with large numbers of variables, while the Nelder-Mead algorithm is very effective in solving minimization problems with few dimensions.

The Nelder-Mead algorithm begins by selecting a simplex of n+1 points (n is the problem dimensionality, in our case, n=2). Mathematically, the selection of n+1 points is based on the fact that the derivative of the objective function which has n variables could be estimated by the n+1 function values through finite differences. There are four operations a) reflection, b) expansion, c)

contraction, and d) shrink for moving the vertices of the simplex until it converges. Reflection moves the location of the worse vertex through the centroid to its opposite side; worst means that the value of the objective function at that vertex is the least desirable. In our minimization problem, the worse vertex is the one with the largest objective value. By reflection, the solution space (the interior of the simplex) moves away from the worse set of values and moves closer to a better set. Expansion doubles the distance from the reflection point to the centroid. Similarly, contraction halves the distance from the reflection point to the centroid. Both the expansion and reflection operations reposition the reflected vertex and thus accelerate the search. If no more acceptable move of the vertex can be identified, the edge facing the best vertex is halved and the two vertices on the same edge move towards the best vertex to shrink and close up the simplex. Once the simplex converges to a stationary point, the optimal solution is found.

The unique features of Nelder-Mead allow it to discover patterns which cannot be immediately obtained from the original specifications, and the simplicity of this method can avoid the pitfalls of other sophisticated approaches. Therefore, it is selected as the algorithm in our study.

5.3 Workflow

The workflow for the DEM registration is divided into three phases: data preparation, data processing, and visualization:

- Data preparation. This phase generates all required input data (slope, aspect, and observed error) for the minimization process. First, the tiled SRTM and NED data were merged separately into a single dataset. Then, the DEMs falling inside the two rectangular study areas, SGM and SMM, were extracted. As the NED data is assumed more accurate, the local slopes and aspects were estimated from NED data. The slope at each pixel cell was defined as the square root of the sum of change rates in both x and y directions over the eight adjacent pixels. Aspect, usually measured in degrees $[0°, 360°]$, is determined from the

inverse tangent of *x* direction change divided by *y* direction change in a 3 by 3 window centered at the pixel to be measured. Besides slope and aspect, the observed errors between SRTM and NED datasets were obtained by subtracting terrain height values on a pixel-by-pixel basis. Finally, these three images were converted to 2-dimensional ASCII matrices as the input for the minimization process.

- Data processing. This phase optimizes the function introduced in Section 5.1 utilizing the Nelder-Mead algorithm. As the premise of this procedure is that misregistrations are uniform in local blocks, the original data matrices were divided up into several blocks, and the shift computed separately in each block. Using 1km*1km as the block size, and considering that we are using 30m DEM data, then Block 1 (right matrix in Figure 4) will contain cells falling in the first 30 rows and 30 columns. Applying the shift model (in Section 5.1) at each pixel and summing over the 900 pixels, we obtained the function to solve for Block 1. Similarly, functions for other blocks can be obtained and the Nelder-Mead minimization can be applied to obtain one local shift vector per block.

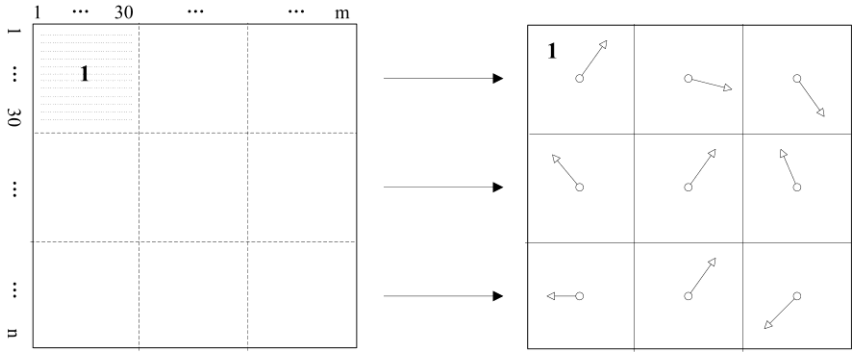

Figure 4. Mapping from original data matrix into matrix of smaller blocks 1km on a side.

- Visualization. Through the above process, we obtained the misregistrations between SRTM and NED for all blocks in terms of shift offset and angle. To visualize the shift in each block on the actual terrain, each such shift vector was added into a polyline shapefile. The start point of each shift vector is the center of the scene. The end point of the shift vector is

calculated from the offset and angle of the shift. As sub-pixel shift is usually small in comparison to the extent of scene, the offset was lengthened by 25 times when being rendered on the map.

6. Results

6.1 Experiment (A): method validation by synthetic data

To validate the proposed method, we constructed a cone-shaped mountain with steep terrain (the slope is 100%) to simulate similar steep terrain in our study area. The mathematical expression of the mountain is known as follows:

$$z = r - \sqrt{(x - x_0)^2 + (y - y_0)^2},$$

Subject to: $x^2 + y^2 \le r^2; x, y \in [-r, r]$

where, (x_0, y_0) is the centroid of the mountain base (a circle) and r is the highest elevation of the synthetic mountain. The characteristic of the cone-shaped mountain is that the slope is always the same but the aspect is always changing. Table 2 shows the spatial profile of the synthetic mountain. After constructing the mountain, a misregistration shift was introduced at 0.5 pixel in the eight directions of north, south, east, west, northeast, southeast, southwest and northwest (Figure 5 shows the shift from original location (colored) to the northwest direction (grey)). Then the observed elevation difference, slope, and aspect at each pixel cell were computed to feed into the Nelder-Mead algorithm for generating the estimated shift. Finally, the estimated shift and the actual shift were compared, giving the results shown in Table 3.

Table 2: Parameters of cone-shaped mountain

Parameter	Notation	Value
Base centroid	(x_0, y_0)	(0,0)
Height	r	2
Slope	θ	100%

Aspect	α	$180 + \arctan(x/y)$, $y > 0$ $360 + \arctan(x/y)$, $x > 0, y < 0$ $\arctan(x/y)$, $x < 0, y < 0$
Pixel size	s	0.01
Relative Shift	$\vec{d}_r$	(2.732 pixel size, 30 °)
Absolute Shift	$\vec{d}_{ab}$	(0.02732, 30 °)
Block size		1 by 1

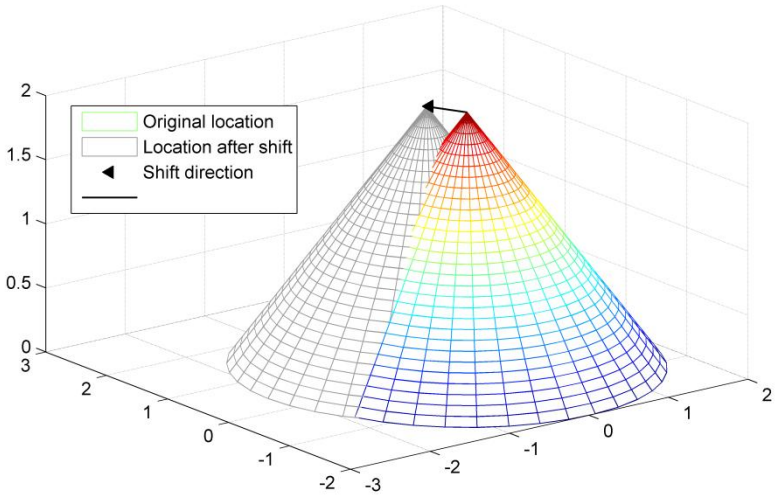

Figure 5. Manual shift of the synthetic mountain.

Table 3 compares the result obtained from the Nelder-Mead estimation and the actual shifts for this mountain. The local shift vectors returned from the Nelder-Mead estimation were averaged to obtain the Estimated Shift. Note that in the determination of this two-dimensional variable (one dimension is the offset and the other is the angle), we rely not only on the values, but also the signs. For example, in case (6), the detected direction of shift was 45 °with negative sign and the detected distance of shift was -0.005, which is also negative. The negative sign of angle means that the direction is 45 °counter clockwise from the North and negative value of the offset means the vector should be reflected to the opposite quadrant. Therefore, the shift should be (0.005,

135 °). By this transformation, we can represent the vector in a uniform manner (no variable has negative value), as shown in Column 5, Table 3.

From Table 3, it can be seen that the proposed Nelder-Mead estimation shows good performance in identifying the shift in eight directions at a sub-pixel (½ pixel) level. Errors in the estimated offset were no more than 2% and errors in shift angle less than 1 °. This experiment proves the validity of the proposed method in handling the co-registration of DEMs with terrains on which aspect changes frequently. We also plotted (Figure 6) the elevation differences averaged over all aspects when the data has misregistration in all cardinal and ordinal directions. These Sin-like curves indicate that the averaged elevation differences maximize at the aspect (direction) of introduced shift. This conclusion can be deduced from the spatial model introduced in Section 5.1 – at the direction of the shift, the elevation difference is toward the steepest slope and therefore, the elevation difference at that direction is maximal. This finding can be used to assess the accuracy of estimated shift from the real datasets.

Table 3. Comparison of estimated result by minimization and actual shift

Case	Shift Direction	Shift distance	Actual Shift	Estimated Shift
(1)	North	½ pixel	(0.005, 0 °)	(0.005, 0.1 °)
(2)	South	½ pixel	(0.005, 180 °)	(0.005, 180.2 °)
(3)	East	½ pixel	(0.005, 90 °)	(0.005, 90 °)
(4)	West	½ pixel	(0.005, 270 °)	(0.005, 269.83 °)
(5)	Northeast	½ pixel	(0.005, 45 °)	(0.0049, 45.78 °)
(6)	Southeast	½ pixel	(0.005, 135 °)	(0.005, 135.02 °)
(7)	Southwest	½ pixel	(0.005, 225 °)	(0.0049, 225.97 °)
(8)	Northwest	½ pixel	(0.005, 315 °)	(0.005, 315.08 °)

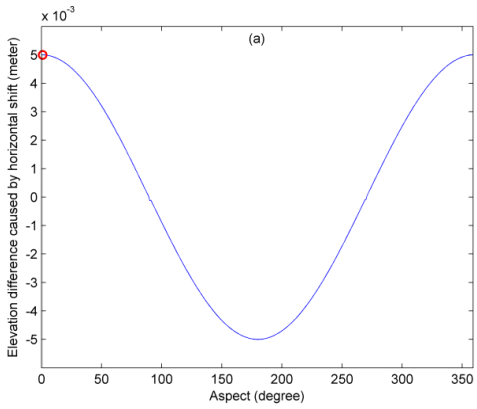
x 10^-3
(a)
Elevation difference caused by horizontal shift (meter)
Aspect (degree)

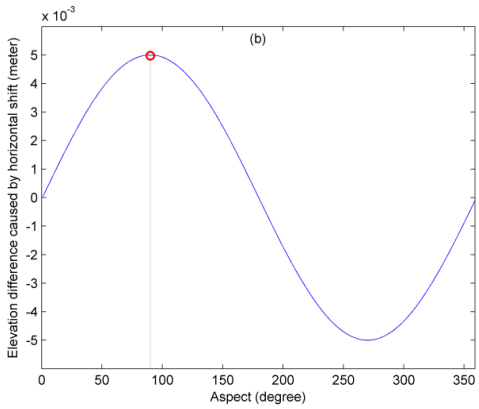
x 10^-3
(b)
Elevation difference caused by horizontal shift (meter)
Aspect (degree)

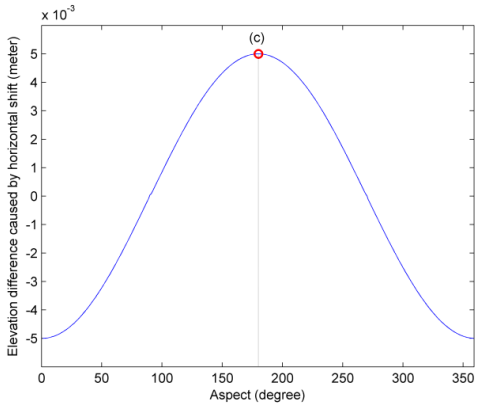
x 10^-3
(c)
Elevation difference caused by horizontal shift (meter)
Aspect (degree)

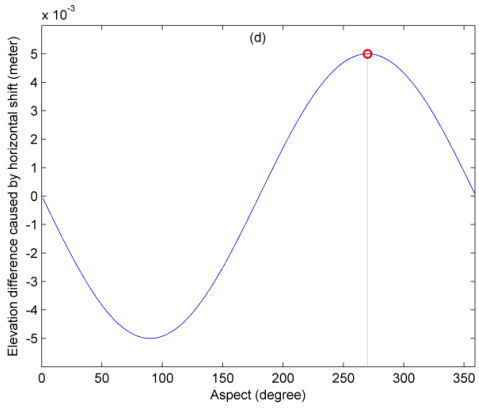
x 10^-3
(d)
Elevation difference caused by horizontal shift (meter)
Aspect (degree)

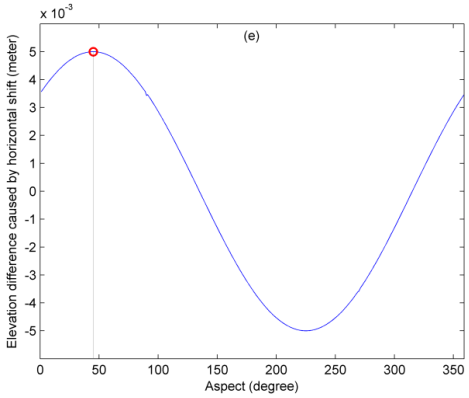
x 10^-3
(e)
Elevation difference caused by horizontal shift (meter)
Aspect (degree)

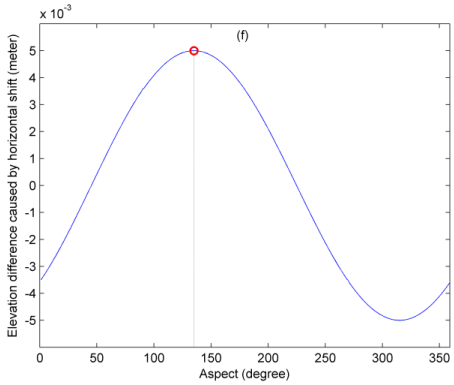
x 10^-3
(f)
Elevation difference caused by horizontal shift (meter)
Aspect (degree)

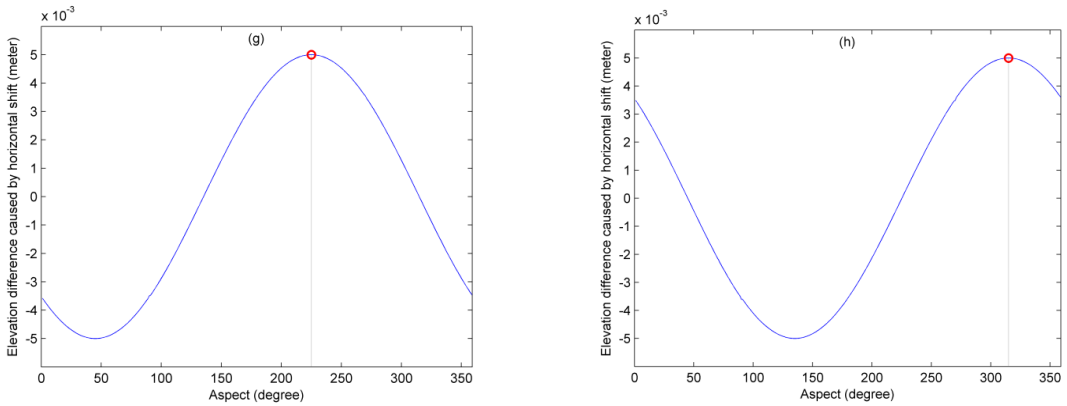

Figure 6. Averages of elevation difference caused by horizontal shift in terms of aspect. (a)-(d) represent cases of the shifts towards four cardinal directions: North, East, South and West. (e)-(h) represent cases of shifts towards four ordinal directions: Northeast, Southeast, Southwest and Northwest.

6.2 Experiment (B): local shift identification in both SGM and SMM regions.

Experiment (A) testified the validity of proposed method in identifying sub-pixel misregistration. This experiment explores the actual shifts that exist between SRTM and NED data in both study sites: SGM (Figure 7a) and SMM (Figure 7b). The block size for both regions is 1.4km*1.4km. The numbers on the arrows refer to the offsets of the shifts and the directions refer to the angle of the shifts. From the figures, we can tell that the SRTM dataset maintains a consistent sub-pixel shift towards Northwest to the NED dataset within both regions. We also found that the offset (25.8 meters) of the shift in the SGM region, although also sub-pixel, is greater than that in SMM region which has less steep terrain.

On average, the shifts are (25.8m, -23.6 °) for the SGM region and (17.89m, -27.6 °) for the SMM region at the tested scale. By using blocks rather than estimating a single shift for each region, we are able to explore the possibility of spatial variations in shifts. We can infer from Figure 7 and the above experiments that the misregistration is a systematic offset in this case, in two continuous terrains that have similar topographical features. However, the misregistration is not a

global offset; its value tends to be larger in steeper terrains (such as the SGM region) and smaller in less steeper terrains (such as the SMM region). Figures 7a and 7b show possibly interesting patterns of variation between the shifts estimated from blocks.

One might argue that the selection of block size in the experiment may affect the results. In order to explore a possible effect, the optimization procedure was performed on fourteen different block sizes: 250m*250m, 500m*500m, 1km*1km, 1.2km*1.2km, 1.4km*1.4km, 1.6km*1.6km. 1.8km*1.8km, 2km*2km, 3km*3km, 4km*4km, 5km*5km, 6km*6km, 7km*7km and study area as a whole. We found that the shifts obtained from different block sizes are all similar, with offset falling in ranges between 24.3 m and 26.6m and angle ranges from -24.5 ° and -23.2 ° in the SGM region. The misregistrations obtained in the SMM region fall between 16.78m and 19.13m of offset and the angle of the shift ranges from -28.78 ° to -26.02 °.

Besides the multi-scale analysis, we also generated a map of the elevation differences between the original SRTM and NED data. Figure 8 shows these differences averaged and plotted by aspect. The peak differences for the SGM region occur when aspect equals 337 ° (23 ° measured counter clockwise from the North) and for the SMM region when aspect equals 332 ° (28 ° counter clockwise from the North). These values are consistent with the shifts (-23.6 ° in SGM region and -27.6 ° in SMM region) identified during the registration procedure. This experiment further verifies the effectiveness of the proposed method in detecting the misregistration.

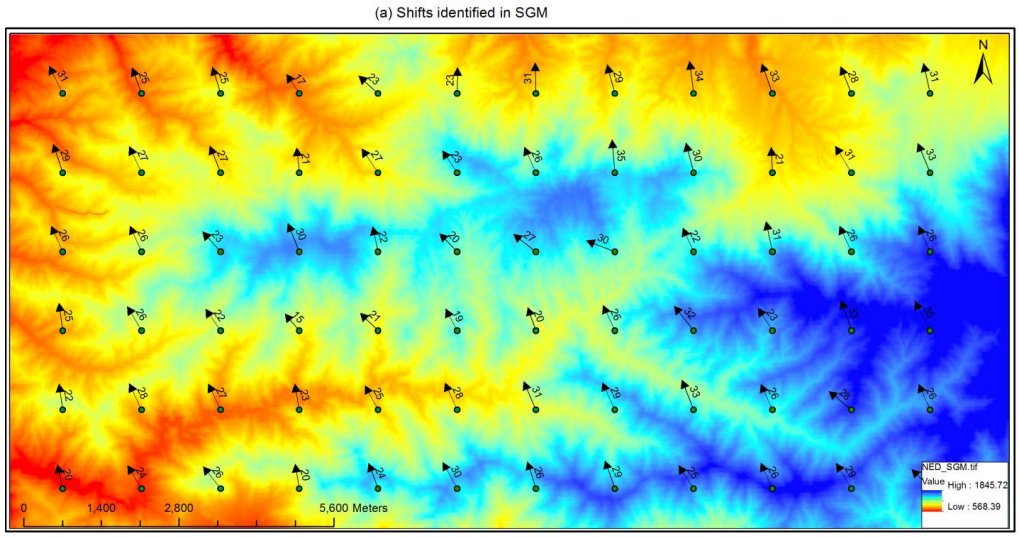

(a)

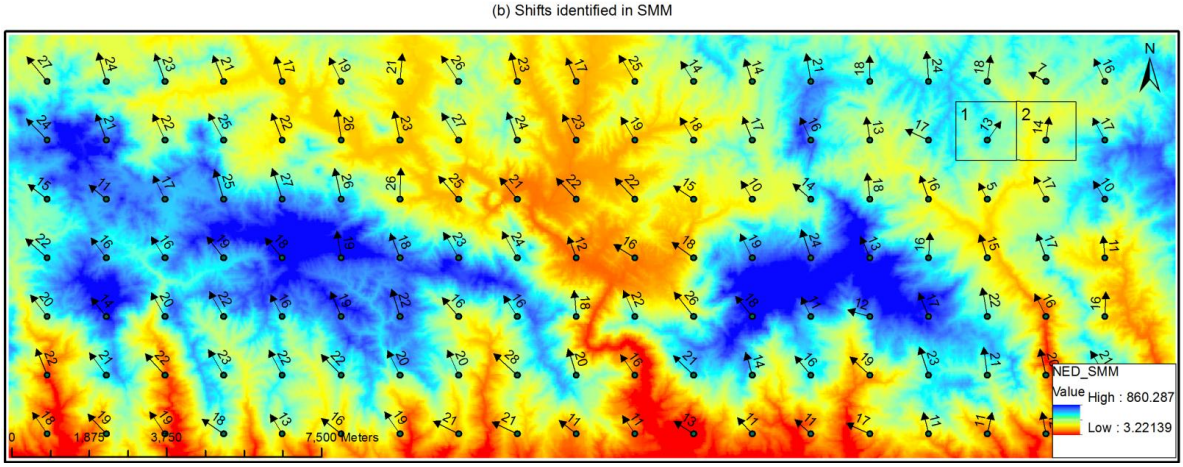

(b)

Figure 7. Visualization of identified shift at 1.4km*1.4km scale from both SGM (a) and SMM (b) regions.

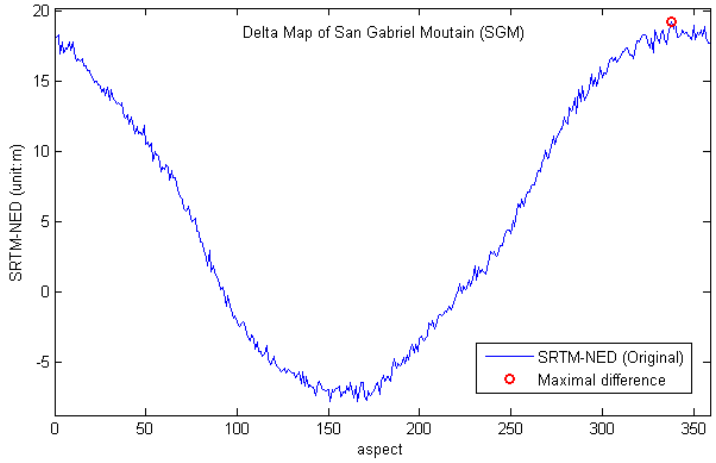

(a)

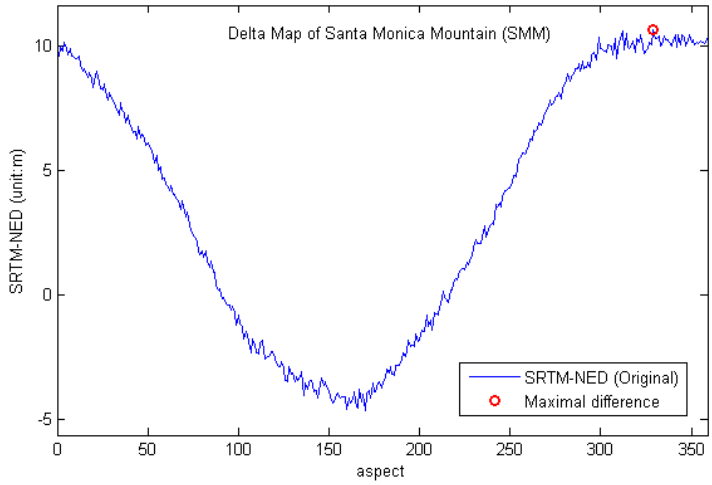

(b)

Figure 8. Average of elevation differences between SRTM and NED plotted against aspect in the SGM (a) and SMM (b) regions.

7. Conclusion and Discussion

This paper presents a robust optimization technique to identify horizontal misregistration between multi-source DEMs. We introduced the formulation of the problem by proposing a shift vector that considers elevation differences, local slope, and aspect. The Nelder-Mead algorithm applied to solve the multidimensional unconstrained nonlinear minimization problem produced satisfying

results through a number of experiments using both synthetic and real dataset in the SGM and SMM regions.

The major contribution of this work is the quantification of horizontal misregistration on a sub-pixel level, which is essential for performing precise science analyses. From the multi-scale analysis, we obtained that the averaged horizontal shift in the SGM region is 25.8 meters with 23.6 ° deviation to the North; for SMM region, the averaged horizontal shift is 17.89 meters with 27.6 ° deviation to the North. We also found that the horizontal misregistration is a systematic offset in continuous terrains that have similar topographical features. However, the misregistration is not a global offset; its value tends to be larger in steeper terrains (such as the SGM region) and smaller in less steep terrains (such as the SMM region).

Technically, one difficulty to overcome in solving the optimization problem is local optimality due to the non-convex nature of this problem. During the experiment, we found some evidence of local optima in some blocks. For example, the original shift identified in the SGM region for the block at row 3 and column 11 was (34.47m, -23.23 °), which implies an overestimation of the offset, given that the averaged shift for the SGM region is (25.8m, -23.6 °). When such indications of a local optimum occurred, the optimization algorithm was rerun on the block by using the average shifts as an initial state. If the new estimates led to a smaller objective function, that is, a better solution, the original local estimates would be replaced. In this way, the local optima could be avoided.

However, after removing the local minima, there remain some anomalies of the shifts. For instance, consider the obviously abnormal shifts identified in two scenes numbered 1 and 2 in the black box in Figure 7(b). By looking into the actual satellite images of both blocks, we found that a substantial portion of the two blocks are developed, and there are large warehouses in Block 1 and many residential buildings in Block 2. The elevation surface containing the heights of the

buildings in the SRTM data is not consistent with the actual terrain surface anymore. Development and other inherent uncertainties in DEM datasets, such as those caused by the coarse resolution, are probably the reason for these anomalies. Nevertheless, using the proposed method, we are still able to produce valid and satisfying results for most of the regions in our study area.

In the future, we will work on quantifying uncertainties that cause the anomalies in the estimation of DEM misregistration, in order to produce more accurate results. Then we will expand this research to detect misregistrations in urban areas. Both of the research directions require an effective mechanism in detecting the locations of human construction, and a method to remove the effects caused by these features in the DSM data. Land-use data indicating the footprint of buildings need to be considered and a more complicated optimization procedure needs to be developed. We will also work on improving the computing performance of the optimization process. For the study areas used in this paper, a single workstation (Intel Core i5 CPU with 2*3.2GHz cores; 8G memory) can finish processing in about 0.2 hours. When dealing with the problem over a much larger extent and with finer-resolution data, a single workstation will be far less satisfying in computing performance. As the optimization is conducted on equally sized regions, it fits naturally the divide-and-conquer paradigm employed in GPGPU (General Purpose Graphic Processing Unit) processing. Therefore, parallelization and optimization of the algorithm, and its adaptation to GPU clusters, will be another focus of our further work.

References

Broyden, C.G., 1965. A class of methods for solving nonlinear simultaneous equations, *Mathematics of Computation*, 19(92): 577–593.

Birgin, E. and Martinez, J.M. 2001. A spectral conjugate gradient method for unconstrained optimization, *Applied Mathematics and Optimization*, 43: 117–128.

Carpenter, J. and Hogarty, J., 2007. Multiple DEM measured accuracy, *Proceedings of ASPRS 2007 Annual Conference, Tampa, Florida*, Article 13.

Celis, M., Dennis, J. E., and Tapia, R. A., 1984. A trust region strategy for nonlinear equality constrained optimization, *Numerical Optimization* (P. Boggs, R. Byrd, and R. Schnabel, editors), SIAM, Philadelphia, pp. 71–82.

Davis, M.H., Khotanzad, A., Flaming, D.P., Harms, S.E., 1997. A physics-based coordinate transformation for 3D image matching, *IEEE Transactions on Medical Imaging*, 16: 317–328.

Dai, X. and Khorram, S., 1998. The effects of image misregistration on the accuracy of remote sensed change detection, *IEEE Transactions on Geoscience and Remote Sensing*, 36: 1566–1577.

Dawn, S., Saxena, V., and Sharma, B., 2010. DEM registration and error analysis using ASCII values, *Proceedings of the International Conference on Signal Processing and Imaging Engineering 2010, San Francisco, USA, 20-22 October*.

Dennis, J. E. and Schnabel, R. B., 1989. A view of unconstrained optimization, *Handbooks in Operations Research and Management Science* (G.L. Nemhauser, A.H.G. Rinnooy Kan, and M.J. Todd, editors), North-Holland, New York, N. Y., vol. 1.

Fan, S.S. and Zahara, E., 2007. A hybrid simplex search and particle swarm optimization for unconstrained optimization, *European Journal of Operational Research*, 181(2): 527–548.

Flusser, J., 1992. An adaptive method for image registration, *Pattern Recognition*, 25: 45–54.

Gesch, D.B., 2007. The National Elevation Dataset. In D. Maune (Ed.), *Digital Elevation Model Technologies and Applications: The DEM Users Manual*. 2nd Edition, ASPRS, Bethesda, MD, pp. 99–118.

Gesch, D.B., Oimoen, M., Greenlee, S., Nelson, C., Steuck, M., and Tyler, D., 2002. The National Elevation Dataset, *Photogrammetric Engineering and Remote Sensing*, 68(1): 5–11.

Goodchild, M.F., Buttenfield, B.P. and Wood, J., 1994. Introduction to visualizing data quality. *Visualization in Geographic Information Systems (*H.M. Hearshaw and D.J. Unwin, editors), John Wiley and Sons, New York, N.Y., pp. 141–149.

Goshtasby, A., 1987. Piecewise cubic mapping functions for image registration, *Pattern Recognition*, 20: 525–533.

Guizar-Sicairos, M., Thurman, S. T., and Fienup, J. R., 2008. Efficient subpixel image registration algorithms, *Optics Letters*, 33(2): 156–158.

Hestenes, M. R. and Stiefel, E., 1952. Methods of conjugate gradients for solving linear systems, *Journal of Research of the National Bureau of Standards*, 49 (6): 409–436.

Huggel, C., Kaab, A., Haeberli, W., and Krummenacher, B., 2003. Regional-scale GIS-models for assessment of hazards from glacier lake outbursts: evaluation and application in the Swiss Alps, *Natural Hazards and Earth System Sciences*, 3: 647–662.

Lewis, R.M., Torczon, V., and Trosset, M.W., 2000. Direct search method: then and now. *Journal of Computational and Applied Mathematics*, 124: 191–207.

Maddalena, D., 2010. Comparison of 30-meter SRTM and NED Data for use in Watershed Delineation and Characteristic Extraction in the Piedmont, North Carolina, Ph.D. dissertation, North Carolina State University, Raleigh, North Carolina, 151p.

Maune, D.F., Maitra, J.B., and McKay, E.J., 2007. Accuracy standards and guidelines. *Digital Elevation Model Technologies and Applications: The DEM User's Manual* (D.F. Maune, editor). 2nd Edition, ASPRS, Bethesda, M.D., pp.61–82.

Miliaresis, G. and Delikaraoglou, D., 2009. Effects of percent tree canopy density and DEM misregistration on SRTM/NED vegetation height estimates, *Remote Sensing*, 1: 36-49.

Neculai, A., 2008. A scaled nonlinear conjugate gradient algorithm for unconstrained optimization, *Optimization*, 57(4): 549–570.

Nelder, J. A. and Mead, R., 1965. A simplex method for function minimization, *Computer Journal*, 7: 308–313.

Reddy, B.S. and Chatterji, B.N., 1996. An FFT-based technique for translation, rotation, and scale-invariant image registration, *IEEE Transactions on Image Processing*, 5: 1266–1271.

Rodr ǵuez, E., Morris, C. S., and Belz, J. E., 2006. A global assessment of the SRTM performance, *Photogrammetric Enginnering & Remote Sensing*, 72(3): 249-260.

Nuth, C. and Kaab, A., 2011. Co-registration and bias corrections of satellite elevation data sets for quantifying glacier thickness change, *The Cryosphere*, 5: 271-290.

Smith, B. and Sandwell, D., 2003. Accuracy and resolution of shuttle radar topography mission data, *Geophysical Research Letters*, 30: 1467.

Sui, D.Z., 2004. Tobler's First Law of Geography: A big idea for a small world, *Annals of the Association of American Geographers*, 94: 269–277.

Townshend, J.R.G., Justice, C.O., Gurney, C. and McManus, J., 1992. The impact of misregistration on change detection, *IEEE Transactions on Geosciences and Remote Sensing*, 30: 1054–1060.

Wolfe, P., 1969. Convergence conditions for ascent methods, *SIAM Review*, 11: 226–235.

Van Niel, T.G., McVicar, T. R., Li, L., Gallant, H. and Yang, Q., 2008. The impact of misregistration on SRTM and DEM image differences, *Remote Sensing of Environment*, 112(2008): 2430-2442.

Zitová, B. and Flusser, J., 2003. Image registration methods: a survey, *Image and Vision Computing*, 21(11): 977-1000.

Zebker, H.A., Werner, C.L., Rosen, P.A. and Hensley, S., 1994. Accuracy of topographic maps derived from ERS-1 interferometric radar, *IEEE Transactions on Geoscience and Remote Sensing*, 32(4): 823-836.